AFRL-RX-WP-TP-2009-4121

ELEMENTAL PARTITIONING ASSOCIATED WITH DIFFERENT GENERATIONS OF GAMMA PRIME PRECIPITATES IN RENE 88DT NICKEL BASE SUPERALLOY (PREPRINT)

J.Y. Hwang, S. Nag, R. Srinivasan, J. Tiley, G.B. Viswanathan, H.L. Fraser, and R. Banerjee

University of North Texas

MARCH 2009

AIR FORCE RESEARCH LABORATORY
MATERIALS AND MANUFACTURING DIRECTORATE
WRIGHT-PATTERSON AIR FORCE BASE, OH 45433-7750
AIR FORCE MATERIEL COMMAND
UNITED STATES AIR FORCE

REPORT DOCUMENTATION PAGE

Form Approved
OMB No. 0704-0188

1. REPORT DATE *(DD-MM-YY)*	2. REPORT TYPE	3. DATES COVERED *(From - To)*
March 2009	Journal Article Preprint	

4. TITLE AND SUBTITLE

ELEMENTAL PARTITIONING ASSOCIATED WITH DIFFERENT GENERATIONS OF GAMMA PRIME PRECIPITATES IN RENE 88DT NICKEL BASE SUPERALLOY (PREPRINT)

5a. CONTRACT NUMBER
FA8650-08-C-5226

5b. GRANT NUMBER

5c. PROGRAM ELEMENT NUMBER
62102F

6. AUTHOR(S)

J.Y. Hwang, S. Nag, and R. Banerjee (University of North Texas)
R. Srinivasan, G.B. Viswanathan, and H.L. Fraser (The Ohio State University)
J. Tiley (AFRL/RXLMD)

5d. PROJECT NUMBER
4349

5e. TASK NUMBER
20

5f. WORK UNIT NUMBER
LM114100

7. PERFORMING ORGANIZATION NAME(S) AND ADDRESS(ES)

University of North Texas
Denton, TX

The Ohio State University
Columbus, OH

Metals Branch (AFRL/RXLMD)
Metals, Ceramics, and NDE Division
Materials and Manufacturing Directorate
Wright-Patterson Air Force Base, OH 45433-7750
Air Force Materiel Command, United States Air Force

8. PERFORMING ORGANIZATION REPORT NUMBER

9. SPONSORING/MONITORING AGENCY NAME(S) AND ADDRESS(ES)

Air Force Research Laboratory
Materials and Manufacturing Directorate
Wright-Patterson Air Force Base, OH 45433-7750
Air Force Materiel Command
United States Air Force

10. SPONSORING/MONITORING AGENCY ACRONYM(S)
AFRL/RXLMD

11. SPONSORING/MONITORING AGENCY REPORT NUMBER(S)
AFRL-RX-WP-TP-2009-4121

12. DISTRIBUTION/AVAILABILITY STATEMENT
Approved for public release; distribution unlimited.

13. SUPPLEMENTARY NOTES
Journal article submitted to *Materials Science and Engineering A*. PAO Case Number: 88 ABW-2009-0066; Clearance Date: 12 Jan 2009. The U.S. Government is joint author of this work and has the right to use, modify, reproduce, release, perform, display, or disclose the work. Paper contains color.

14. ABSTRACT

The compositional and microstructural evolution of different generations of precipitates of the ordered γ' phase during the continuous cooling, followed by isothermal aging, of a commercial nickel base superalloy, Rene 88DT, has been characterized by three dimensional atom probe tomography (3DAP) coupled with energy-filtered transmission electron microscopy studies. After solutionizing in the single γ phase field, during continuous cooling at a relatively slow rate (~ 24°C/min), the first generation primary γ' precipitates, forming at relatively higher temperatures, exhibit near-equilibrium compositions, while the smaller scale secondary γ' precipitates, forming at lower temperatures, exhibit non-equilibrium compositions often consisting of excess Co and Cr, while being depleted in Al and Ti content. The compositions of the γ matrix near these precipitates also exhibit similar trends with the composition being closer to equilibrium near the primary precipitates as compared to the secondary precipitates.

15. SUBJECT TERMS
compositional, isothermal, nickel base superalloy, Rene 88DT

16. SECURITY CLASSIFICATION OF:			17. LIMITATION OF ABSTRACT:	18. NUMBER OF PAGES	19a. NAME OF RESPONSIBLE PERSON (Monitor)
a. REPORT	b. ABSTRACT	c. THIS PAGE			Jay Tiley
Unclassified	Unclassified	Unclassified	SAR	32	19b. TELEPHONE NUMBER *(Include Area Code)* N/A

Standard Form 298 (Rev. 8-98)
Prescribed by ANSI Std. Z39-18

Elemental Partitioning Associated with Different Generations of Gamma Prime Precipitates in Rene 88DT Nickel Base Superalloy

J. Y. Hwang, S. Nag, R. Srinivasan[#], J. Tiley*, G. B. Viswanathan[#], H. L. Fraser[#], and, R. Banerjee

Center for Advanced Research and Technology and
Department of Materials Science and Engineering
University of North Texas, Denton, Texas, U. S. A.

[#]Center for the Accelerated Maturation of Materials and
Department of Materials Science and Engineering
The Ohio State University, Columbus, Ohio, U. S. A.

*Materials and Manufacturing Directorate
Air Force Research Laboratory, Dayton, Ohio, U. S. A.

Abstract

The compositional and microstructural evolution of different generations of precipitates of the ordered γ' phase during the continuous cooling, followed by isothermal aging, of a commercial nickel base superalloy, Rene 88DT, has been characterized by three dimensional atom probe tomography (3DAP) coupled with energy-filtered transmission electron microscopy studies. After solutionizing in the single γ phase field, during continuous cooling at a relatively slow rate (~ 24°C/min), the first generation primary γ' precipitates, forming at relatively higher temperatures, exhibit near-equilibrium compositions, while the smaller scale secondary γ' precipitates, forming at lower temperatures, exhibit non-equilibrium compositions often consisting of excess Co and Cr, while being depleted in Al and Ti content. The compositions of the γ matrix near these precipitates also exhibit similar trends with the composition being closer to equilibrium near the primary precipitates as compared to the secondary precipitates. Subsequent isothermal aging at 760°C, while leading to some coarsening of the primary γ' precipitates, does not affect their composition to any significant degree. In contrast, the composition of the secondary γ' precipitates is driven towards equilibrium during the isothermal aging.

Introduction

Due to the excellent balance of properties exhibited by nickel base superalloys, both at room as well as elevated temperatures, they have widespread application in a number of critical technological areas, especially those involving high temperatures such as aircraft jet engines. These alloys typically consist of precipitates of the ordered γ' phase (in some cases both γ' and γ'' phases) distributed within a disordered γ matrix. The microstructure of these alloys, especially in terms of the composition, morphology, spatial, and, size distributions of the γ' precipitates plays a very important role in determining the mechanical properties of these alloys [1]. Rene' 88 DT alloy is a recently developed nickel base superalloy that was developed [2-4] to be more damage tolerant than the previous generation Rene' 95 alloy, while offering improved creep strength and fatigue crack growth resistance [4]. The nominal chemistry for this alloy is: 13% Co, 16% Cr, 4% Mo, 4% W, 2.1% Al, 3.7 % Ti, 0.7% Nb, 0.03% C and 0.015% B. This alloy is typically processed through the powder metallurgy route and develops a polycrystalline microstructure consisting of γ grains with nanoscale γ' precipitates. Furthermore, the typical heat-treatment used for this alloy consists of a solutionizing procedure for 30 to 60 minutes at 1150°C (2100°F) in the single γ phase field, followed by continuous cooling to room temperature at appropriate cooling rates, and subsequent aging for different time periods at temperatures such as 760°C (1400°F).

The microstructural evolution in superalloys, such as Rene 88DT, during continuous cooling is strongly dependent on the cooling rate employed. Faster cooling rates, such as those encountered in water quenching the alloy from the high temperature single γ phase field, typically lead to the formation of a monomodal size distribution of refined γ' precipitates [5]. In contrast, relatively slower cooling rates lead to the formation of γ' precipitates of two (bimodal size distribution) or even more different size ranges [5]. During continuous cooling, nucleation events occurring at different undercoolings below the γ' solvus temperature, typically result in the multiple size distributions of γ' precipitates. The first burst of nucleation, occurring at lower undercoolings (or higher temperatures, just below the γ' solvus temperature), lead to the formation of the first generation of γ' precipitates, often referred to as primary γ' precipitates. Similarly, a second burst of nucleation, at higher undercoolings, leads to the formation of secondary γ' precipitates and there might be additional bursts of nucleation at even lower temperatures [5]. They have been a number of studies employing three dimensional atom probe (3DAP) tomography to characterize the evolution of microstructure in Ni-base superalloys at the nanometer scale, and these studies have been extensively reviewed in recent articles in the published literature [6-8]. The primary emphasis of these studies has been the determination of the size, morphology, and, composition of the γ' precipitates within the γ matrix during the early stages of precipitation in these alloys during annealing after rapid quenching the alloy from the high temperature single γ phase field. Therefore, typically these studies have focused on a monomodal size distribution of refined γ' precipitates within the disordered γ matrix. In addition, such 3DAP studies have also focused on the partitioning of the alloying additions between these two phases and the segregation of certain alloying additions to interphase (γ/γ' interface) as well as to

grain boundaries.

In case of typical industrially relevant heat-treatments, the cooling rates employed after solutionizing/homogenizing in the single γ phase field are substantially slower than water-quenching and therefore often lead to the formation of multiple size ranges of γ' precipitates. Therefore, the focus of the current paper is on determining the composition of γ' precipitates of different size ranges forming during continuous cooling of Rene 88DT, the compositional partitioning between these γ' precipitates and the adjoining γ matrix, as well as the changes in these compositions during subsequent isothermal aging heat treatments. The elemental partitioning as well as the 3D morphology has been primarily characterized by 3DAP tomography and these studies have been complemented with energy-filtered transmission electron microscopy (EFTEM) studies. While LEAP tomography affords a nanometer scale resolution of structure and chemistry, it offers limited information in terms of the sampled volume of reconstruction. In order to better understand the overall representative morphological features over larger length scales, EFTEM has been found to be a suitable and direct method [9], serving to also confirm the size and morphology of the γ' precipitates as studied through 3DAP tomography. The three primary objectives of this paper are as follows:

1. Investigate the differences in elemental partitioning between the γ matrix and the primary versus secondary γ' precipitates in Rene 88DT, during continuous cooling at a relatively slow rate post a high temperature homogenization treatment in the single γ phase field.
2. Investigate the changes in the composition of the primary and secondary γ' precipitates and the adjoining γ matrix during isothermal heat treatments at 760°C post continuous cooling.

Experimental Procedure

The bulk chemical composition of the commercially procured Rene 88 DT alloy was 56.53Ni-16.24Cr-13.27Co-3.92Ti-2.09Al-4.08Mo-3.92W-0.76Nb (wt%) or 55.63Ni-18.02Cr-13.00Co-4.74Ti-4.45Al-2.48Mo-1.21W-0.46Nb (at%). Material was cut from the bore and rim section of a turbine disk, produced and tested under a DARPA program [10]. The samples were supersolvus solution treated in a vacuum furnace at 1150°C in the single γ phase field for 30 minutes to dissolve any existing γ' and then slow cooled at an average cooling rate of 24^0C/min. These samples were subsequently aged for 0, 50, and, 200 hours at 760°C in a large chamber vacuum furnace and air quenched. For convenience, these samples will be subsequently referred to as SC0, SC50, and, SC200 samples in the remaining part of this paper.

Samples for 3DAP tomography studies in the LEAP microscope were prepared by a combination of electro-polishing and focused ion beam milling techniques. For this purpose, samples from the different heat-treated conditions were first electro-discharge machined into thin wires with a square cross section (~ 0.5 x 0.5 mm). These wires were mechanically ground and subsequently electro-polished to tip diameters ~ 1 μm using a commercially available Electropointer™ system. The electro-polishing was carried out in

two steps, first with a 95% acetic acid + 5% perchloric acid solution using 25 V for the coarser polish and finally with an 98% butyl cellulose + 2% perchloric acid solution using 10V for the final polish. These electro-polished needles were subsequently thinned further in a dual-beam focused ion beam (FIB) instrument (FEI Nova Nanolab 200) system using a Ga ion beam. The ion beam thinning was carried out in multiple steps, starting with 30 kV ions and finally finishing with 5 kV ions to reduce the surface damage caused by the higher energy ions [11]. The final tip diameter of the atom probe specimens was ~ 50 – 80 nm. The 3DAP experiments were carried out using a LEAP 3000 local electrode atom probe (LEAP™) system from Imago Scientific Instruments Inc. All atom probe experiments were carried out in the electric-field evaporation mode at a temperature of 70K, with the evaporation rate varying from 0.2 – 1.0 % and the pulsing voltage at 30% of the steady-state applied voltage.

TEM samples were also prepared via conventional routes, consisting of mechanical grinding and polishing of 3 mm diameter discs, followed by dimple grinding, and, final ion-beam milling to electron transparency. Ion beam milling was conducted on a Gatan Duo Mill and Fischione Model 1010 ion milling system, operated at 6 kV. TEM analysis was conducted on a FEI Tecnai F20 field emission gun transmission electron microscope operating at 200 KV. Images were obtained using the Cr M-edge in the energy filtered transmission electron microscopy (EFTEM) mode, as described elsewhere [12]. Representative regions were imaged at different magnifications to capture the relevant secondary and/or tertiary γ' precipitates in the alloy.

Results and Discussion

As slow-cooled (SC0) sample

Energy-filtered TEM images, acquired using the Cr M-edge for the slow-cooled SC0 sample (without any additional aging) are shown in Figs. 1(a) and (b). The regions exhibiting a darker contrast in these images, arising from Cr depletion, correspond to the γ' precipitates. There is a clear difference between the two size scales of γ' precipitates visible in these images leading to a bimodal distribution of precipitate sizes. The larger of these correspond to the primary γ' precipitates exhibiting highly irregular morphologies while the smaller ones are the secondary γ' precipitates exhibiting a near spherical morphology with a tendency towards flattening of the edges with coarsening. Furthermore, as clearly visible in Fig. 1(b), there appears to be γ'-depleted zone, similar to a precipitate-free zone, separating the primary γ' precipitates from the secondary γ' precipitates. Within this zone, there are either no γ' precipitates, or a substantially reduced density of highly refined γ' precipitates, not visible at the resolution of the EFTEM images shown in Fig. 1(b).

Fig. 2 shows the 3DAP data from one of the larger primary γ' precipitates in the SC0 sample. It should be noted that the large size scale of the primary γ' precipitates in these samples makes it impossible to capture an entire precipitate within the rather limited field of view of an atom probe sample. Fig. 2(a) shows a 40 nm x 40 nm x 250 nm reconstruction of the Al ions (in red) and Cr ions (in blue) from the SC0 sample. The Al-rich region, corresponding to the primary γ' precipitate and the Cr-rich region, corresponding to the γ matrix, have been marked on the same figure for clarity. The

compositions of these two phases have been determined by averaging over the ions within spherical zones, such as the one marked in Fig. 2(a). Thus, the average composition has been determined for the primary γ' precipitate and is listed in Table I. The composition of the γ matrix was determined at two different locations, one near the interface with the primary γ' and the second one away from the precipitate. Both these compositions have been listed in Table II. Based on the results shown in Tables I and II for the primary γ' and γ compositions, it can be concluded that in Rene 88DT, while Al and Ti segregate preferentially to the γ' phase, Cr, Co, and, Mo segregate to the γ matrix. In addition, the composition profiles, for the primary elements of interest in Rene 88DT, has also been determined across the γ/γ' interface, especially focusing on the change in the composition of the γ matrix moving away from the interface. These composition profiles have been determined by averaging across a cylinder of 5 nm diameter, shown in Fig. 2(b). The actual composition profiles for Cr, Co, Al, Ti, and Mo, are shown in Fig. 2(c). The reason for investigating the long range change in γ composition as a function of distance from the primary γ'/γ interface is to address the possible reasons underlying the formation of a γ'-depleted zone near these primary precipitates. Similar studies were carried out on the smaller scale secondary γ' precipitates, the results of which have been summarized in Fig. 3 and Tables I and II. Fig. 3 shows a 50 nm x 50 nm x 40 nm 3DAP reconstruction from the same SC0 sample, showing Al ions in red and a Cr isoconcentration surface (also referred to in short as isosurface) for Cr = 14at% in blue. The Cr isosurface allows for a clear delineation between the γ' and γ regions within the 3DAP reconstruction, based on the compositional partitioning with the Cr-depleted regions corresponding to the γ' precipitates [12]. The reconstruction shown in Fig. 3 captures the small edge section of a primary γ' precipitate, a number of smaller secondary γ' precipitates, and the γ'-depleted zone separating them. The compositions of two different secondary γ' precipitates from this reconstruction have been listed in Table I, while the composition of the γ matrix near the secondary γ' precipitates has been listed in Table II.

Referring to Table I, there appear to be significant differences between the compositions of the primary and secondary γ' precipitates in the SC0 sample. More specifically, considering the elements segregating to the γ' phase, while the Ti content is less in the secondary precipitates as compared to the primary precipitate, the Al content appears to be quite similar. Comparing the elements tending to segregate to the γ matrix, for all the three elements, Cr, Co, and, Mo, the secondary precipitates exhibit a higher concentration as compared to the primary precipitate. These results clearly indicate that in the as slow-cooled condition, the primary γ' precipitates are able to achieve a composition closer to equilibrium as compared to the secondary γ' precipitates. These differences in compositions between the primary and secondary γ' precipitates is evidence in favor of the fact that these two generations of precipitates formed at different undercoolings. Thus, while the primary γ' precipitates formed at a higher temperature, the higher diffusivities of the alloying elements at that temperature permitted these precipitates to reach closer to an equilibrium condition. In contrast, the secondary γ' precipitates formed at a lower temperature, where presumably the lower diffusivities of the alloying elements

restricted the partitioning of these elements between the γ and γ' phases, resulting in far-from equilibrium compositions of the secondary γ' precipitates.

Composition of the γ matrix in the vicinity and far from the primary γ' precipitates as well as near the secondary γ' precipitates exhibits some interesting differences as shown in Table 2. Thus, the γ near the primary γ' precipitate exhibits a substantially higher content of Co as compared to far from the precipitate. The other primary alloying elements, Cr, Al, Ti, and, Mo, appear to have almost the same concentrations both near as well as far from the primary γ' precipitate. The higher concentration of Co near the primary γ'/ γ interface is also clearly visible in the Co compositional profile shown in Fig. 2(c). These results clearly indicate the possibility of a pile-up of Co in the γ matrix near the growing/coarsening primary γ' precipitate. This would suggest that Co possibly has a lower diffusivity in the matrix as compared with the other alloying elements under consideration, Cr, Al, Ti, and, Mo. The binary interdiffusivity values of Co, Cr, Al, and, W, in the *fcc* Ni matrix at a temperature of 727°C (1000K) are 4.6×10^{-19}, 6.3×10^{-19}, 2.6×10^{-18}, and, 9.2×10^{-19} m^2/s respectively [Smithell's ref]. Based on these values it appears that Co could have the lowest diffusivity in the γ matrix and consequently could be the reason underlying the local pile-up of Co near the primary γ'/ γ interface. Referring to Table 2, the γ near the secondary γ' precipitates exhibits a higher content of Ti and Al and a lower content of Co as compared to the γ near the primary γ' precipitates. This indicates that the γ near the secondary γ' precipitates has not achieved its equilibrium composition and still retains a supersaturation of γ' forming elements Al and Ti. This result indicates that the equilibrium volume fraction of γ' has presumably not yet formed in the SC0 sample and that secondary γ' precipitates are still in their growth phase. In contrast, the γ near the primary γ' precipitates has reached its equilibrium composition while the composition far from these primary precipitates is still not at equilibrium. Therefore, while there is a local chemical driving force for precipitation of γ' in the vicinity of the secondary γ' precipitates, there is either no or only a very limited local driving force for the precipitation of γ' near the primary precipitates. These post-mortem results in the SC0 sample can help explain the formation of the γ'-depleted zone. Thus, during the continuous cooling process, initially the primary γ' precipitates nucleate and grow, at relatively higher temperatures, within the γ matrix. Due to the high temperatures involved, the diffusivities of the alloying elements are relatively high allowing for a rapid short-range partitioning of the alloying elements between the γ and γ' phases. However, since the sample is continuously cooling, there is not sufficient time for the long-range composition to be equilibrated within the γ matrix. Consequently, a non-equilibrium far-field composition is retained within the γ matrix between the growing primary γ' precipitates. On further cooling, at a lower temperature, a second burst of nucleation takes place in these γ regions, in between and far from the existing primary γ' precipitates. This new burst of nucleation results in the formation of the secondary γ' precipitates which are of a substantially refined scale as compared to the primary γ' precipitates.

Slow-cooled followed by 50 hrs aged (SC50) sample

Energy-filtered TEM images, acquired using the Cr M-edge for the SC50 sample, aged for 50 hrs at 760°C following slow-cooling are shown in Figs. 4(a) and (b). There is marginal increase in the size of the primary γ' precipitates and a more substantial increase in the size of the secondary γ' precipitates after isothermal aging for 50 hrs. The γ'-depleted zones, surrounding the primary γ' precipitates are also visible in these EFTEM images, more clearly in the higher magnification image shown in Fig. 4(b).

A 30 nm x 30 nm x 200 nm 3DAP reconstruction showing Al ions in red and Cr isosurface for 14 at% is shown in Fig. 5(a). As discussed in case of the SC0 sample, the Cr isosurface allows for a clear delineation of the γ/γ' interface. The reconstruction shown in Fig. 5(a) contains a section of a large primary γ' precipitate as well as some sections of smaller secondary γ' precipitates. The compositional profiles for Cr, Co, Al, Ti, and, Mo averaged across a cylinder of diameter 5 nm are shown in Fig. 5(b). The corresponding cylinder has been marked in Fig. 5(a). Since this reconstruction only contains small fractions of secondary γ' precipitates, and that too at the very edges of the reconstruction, it is rather difficult to accurately determine the composition of these secondary precipitates. A different 3DAP reconstruction from the same SC50 sample, of dimensions 30 nm x 30 nm x 120 nm, is shown in Fig. 6. This reconstruction contains substantial portions of secondary γ' precipitates, allowing for a more accurate and representative determination of the composition of these precipitates. The compositions of the primary γ' precipitate (shown in Fig. 5(a)) and two of the secondary γ' precipitates (shown in Fig. 6) have been listed in Table 3. The compositions of the γ matrix, near and far from the primary γ' precipitate, as well as near the secondary γ' precipitates, have been listed in Table 4.

From Table 3, comparing the compositions of the primary γ' and the two secondary γ' precipitates, it is apparent that there are no major differences between the compositions of these two types of precipitates after isothermal aging at 760°C for 50 hours. Only subtle differences, such as a marginally lower Ti content and a marginally higher Cr content in the secondary γ'1 precipitate can be observed in this case. This clearly indicates that isothermal aging post slow-cooling has equilibrated the composition of the secondary γ' precipitates in this alloy. Comparing the compositions of the γ matrix (shown in Table 4) near and far from the primary γ' precipitates, it is evident that the higher concentration of Co in the γ matrix near these primary precipitates as compared to the far-field composition, observed in case of the SC0 sample, still persists to a certain degree in the SC50 sample. This is also visible in the compositional profile for Co shown in Fig. 5(b) wherein a marginally higher Co concentration can be seen in the γ near the primary γ' precipitate. These results indicate that while the isothermal aging at 760°C for 50 hours is sufficient for equilibrating the compositions of the secondary γ' precipitates, which involves short-range diffusion, this time period of aging is still not sufficient for equilibrating the composition of the γ matrix, which involves long-range diffusion. Finally, from Table 4 it appears that the composition of γ near the primary γ' is very similar to that near the secondary γ' precipitates, with marginal differences in the Co concentration. This again suggests that locally, both the secondary γ' and the γ adjacent to it are able to achieve near equilibrium compositions due to sufficient time for short-range

diffusion, while the longer-range equilibration has still not taken place in the SC50 sample.

Slow-cooled followed by 200 hrs aged (SC200) sample

Energy-filtered TEM images, acquired using the Cr M-edge for the SC200 sample, aged for 200 hrs at 760°C following slow-cooling are shown in Figs. 7(a) and (b). Again, there is only a marginal increase in the size of the primary γ' precipitates and a more substantial increase in the size of the secondary γ' precipitates as compared to the SC50 sample. The γ'-depleted zones, surrounding the primary γ' precipitates are also visible in these EFTEM image shown in Fig. 7(a).

A 30 nm x 30 nm x 140 nm 3DAP reconstruction of the SC200 sample is shown in Fig. 8(a) with the Al ions colored red and the 14 at% Cr isosurface colored in blue. In this reconstruction, there is a small section of a primary γ' precipitate at the right hand edge of the reconstruction (refer to Fig. 8(a)). Moving towards the left from this primary γ' precipitate, there is first a γ'-depleted region, and then the secondary γ' precipitates are clearly visible in the left hand half of this reconstruction. As clearly visible in Fig. 8(a), the secondary precipitates are also of different size ranges, suggesting that some of the very small γ' precipitates might have formed from fresh nucleation during the isothermal aging at 760°C. The compositional profiles for Cr, Co, Al, Ti, and, Mo, averaged across a cylinder of 5 nm diameter (shown in Fig. 8(a)) are shown in Fig. 8(b). It is evident from these compositional profiles that the long-range γ composition has equilibrated for all the major alloying additions after isothermal annealing at 760°C for 200 hours in the SC200 sample.

The compositions for primary and secondary γ' precipitates in the SC200 sample have been listed in Table 5. It should be noted that since the volume fraction of the primary γ' precipitate captured within the 3DAP reconstruction (Fig. 8(a)), is rather limited, it was difficult to get an accurate composition for the primary precipitate. This possibly resulted in the marginally higher Co content in the primary γ' precipitate of the SC200 sample as compared with the SC0 and SC50 samples. However, the compositions of both the secondary γ' precipitates in the SC200 sample appear to be almost the same and presumably near the equilibrium composition for the γ' phase at the aging temperature of 760°C. There is possibly only a marginally lower Ti content in the secondary γ' precipitates as compared with the primary γ' precipitate. The γ compositions near and far from the primary γ', and near the secondary γ' precipitates, are listed in Table 6. All the three γ compositions listed in this Table appear to almost identical. This is clear evidence of the fact that the matrix composition has equilibrated and homogenized after 200 hours aging at 760°C. It should be noted that the Co concentration is virtually identical near the primary γ' precipitate as well as far-field from the same precipitate, unlike the substantial difference between these values, observed in case of the SC0 and SC50 samples. Therefore, it can be concluded that the long-range diffusive processes have allowed for the homogenization of the composition across the γ matrix in this alloy.

Summary and Conclusions

The solid-state formation of different generations of γ' precipitates within the γ matrix of a commercial Rene 88DT alloy during continuous slow-cooling and subsequent isothermal aging at 760°C for 0, 50, and, 200 hours, has been studied using 3DAP tomography. The focus of the study has been on investigating the partitioning of primary alloying elements, Cr, Co, Al, Ti, and, Mo, between the γ matrix and primary as well as secondary γ' precipitates. The results can be summarized as follows:

1. There is a substantial difference between the compositions of the larger primary γ' precipitates and the smaller secondary γ' precipitates in case of the as slow-cooled SC0 sample. As compared to the primary γ' precipitates, the secondary γ' precipitates contain a larger amount of Cr, Co, and Mo, and a smaller amount of Al and Ti. This difference gradually disappears on isothermal aging at 760°C.
2. There is a substantial difference between the compositions of the γ matrix near and far from the primary γ' precipitates in both SC0 and SC50 samples. This difference is primarily manifested by a larger local concentration of Co in the γ near the primary γ' precipitates which decreases with increasing distance from the primary precipitate. Co appears to be the slowest diffusing alloying element in the γ matrix of Rene 88DT at 760°C. Isothermal aging for 200 hours at 760°C homogenizes the composition of the matrix and obliterates the concentration gradient in Co within the γ matrix.
3. The limited long-range diffusion of primary alloying elements such as Co which are rejected from the growing primary γ' precipitates, results in a concentration gradient near these primary precipitates leading to the formation of γ'-depleted zones. Such zones are clearly visible in all three samples, SC0, SC50, and, SC200.

Acknowledgements

The authors would like to acknowledge the U. S. Air Force Research Laboratory (AFRL ISES contract) and the U. S. Air Force Office of Scientific Research (AFOSR Grant # FA9550-06-1-0193) for providing financial support for this study. In addition, the authors also gratefully acknowledge the Center for Advanced Research and Technology (CART) at the University of North Texas and the Center for the Accelerated Maturation of Materials (CAMM) at the Ohio State University for access to the experimental facilities used for this study.

References

1. R. J. Mitchell, M. Preuss, Metall. Mater. Trans. A, 2007, vol. 38, pp. 615-27.
2. D. D. Krueger, R. D. Kissinger, R. D. Menzies, and, C. S. Wukusick, *U. S. Patent* 4,957,567.
3. D. D. Krueger, R. D. Kissinger, and, R. D. Menzies, *Superalloys 1992*, Ed. S. D. Antolovich et. al., TMS-AIME, Warrendale, PA, 1992, pp. 277-86.
4. S. T. Wlodek, M. Kelly, and, D. A. Alden, *Superalloys 1996*, Ed. R. D. Kissinger, D. J. Deye, D. L. Anton, A. D. Cetel, M. V. Nathal, T. M. Pollock, and, D. A. Woodford, TMS, Warrendale, PA, 1996, pp.129-36.
5. S.S. Babu, M.K. Miller, J.M. Vitek, S.A. David, Acta Mater. 49(2001)4149.
6. D. N. Seidman, C. K. Sudbrack, and, K. E. Yoon, *JOM*, December 2006, pp. 34-9.
7. M. K. Miller, *Micron*, 2001, vol. 32, pp.757-64.
8. D. Blavette, E. Cadel, and, B. Deconihout, *Mater. Char*. 2000, vol. 44, pp.133-57.
9. P. M. Sarosi, G. B. Viswanathan, D. Whitis, and, M. J. Mills, Ultramicroscopy, 2005, vol. 103, pp. 83-93.
10. DARPA program reference.
11. K. Thompson, D. Lawrence, D. J. Larson, J. D. Olson, T. F. Kelly, and, B. Gorman, *Ultramicroscopy*, 2007, vol.107, pp. 131.
12. J.Y. Hwang, R. Banerjee, J. Tiley, R. Srinivasan, G. B. Viswanathan, H. L. Fraser, (Met. Mater. Trans. A, in press, 2008).

Tables

SC0	Primary γ’		Secondary γ’1		Secondary γ’2	
	Atomic %	**Error %**	**Atomic %**	**Error %**	**Atomic %**	**Error %**
Ni	65.18	0.70	55.75	3.67	52.01	4.60
Co	6.70	0.18	8.70	1.21	10.99	1.81
Ti	9.17	0.21	7.14	1.09	6.43	1.35
Cr	1.77	0.09	8.23	1.18	11.53	1.86
Al	9.03	0.21	9.94	1.30	9.38	1.66
Nb	2.87	0.12	2.48	0.63	3.22	0.94
Mo	2.84	0.11	5.12	0.91	4.02	1.06
C	0.55	0.05	0.00	0.00	0.00	0.00
W	1.31	0.08	2.64	0.65	1.88	0.72
B	0.57	0.05	0.00	0.00	0.54	0.38

Table 1: The primary and secondary γ’ compositions for the SC0 sample.

SC0	γ near primary γ’		γ far from prima γ’		γ near secondary γ’	
	Atomic %	**Error %**	**Atomic %**	**Error %**	**Atomic %**	**Error %**
Ni	43.62	0.52	49.57	0.54	44.73	2.33
Co	18.63	0.31	13.71	0.25	15.38	1.22
Ti	0.68	0.05	1.21	0.07	2.68	0.48
Cr	24.36	0.36	24.51	0.35	23.75	1.57
Al	1.97	0.09	1.67	0.08	3.76	0.57
Nb	2.26	0.10	0.97	0.06	2.17	0.43
Mo	5.08	0.15	5.34	0.15	5.02	0.66
C	0.57	0.05	0.44	0.04	0.17	0.12
W	2.24	0.10	2.07	0.09	2.26	0.44
B	0.59	0.05	0.51	0.05	0.08	0.08

Table 2: The γ compositions near and far from primary γ’, and near secondary γ’ precipitates for the SC0 sample.

SC50	Primary γ‘(avg)		Secondary γ’1		Secondary γ’2	
	Atomic %	Error %	Atomic %	Error %	Atomic %	Error %
Ni	62.25	2.58	63.43	5.36	62.51	1.76
Co	6.52	0.68	7.20	1.46	6.13	0.45
Ti	9.22	0.81	8.31	1.58	9.73	0.57
Cr	1.71	0.34	3.32	0.98	1.95	0.25
Al	12.32	0.95	13.02	2.02	12.51	0.66
Nb	3.10	0.46	1.94	0.74	3.54	0.33
Mo	2.96	0.45	1.94	0.74	2.10	0.26
C	0.26	0.13	0.00	0.00	0.09	0.05
W	1.19	0.28	0.55	0.39	1.31	0.20
B	0.46	0.17	0.28	0.28	0.12	0.06

Table 3: The primary and secondary γ’ compositions for the SC50 sample.

SC50	γ near primary γ'		γ far from prima γ'		γ near secondary γ'	
	Atomic %	**Error %**	**Atomic %**	**Error %**	**Atomic %**	**Error %**
Ni	43.43	2.50	41.97	2.06	40.69	1.42
Co	19.26	1.52	15.48	1.13	17.59	0.85
Ti	0.80	0.28	1.56	0.34	0.60	0.15
Cr	23.27	1.70	24.64	1.48	27.94	1.12
Al	2.71	0.53	3.62	0.52	2.51	0.30
Nb	1.20	0.35	2.27	0.41	1.62	0.24
Mo	6.52	0.83	6.25	0.69	5.90	0.47
C	0.60	0.25	1.14	0.29	0.39	0.12
W	1.71	0.42	2.27	0.41	2.23	0.28
B	0.50	0.22	0.78	0.24	0.53	0.14

Table 4: The γ compositions near and far from primary γ', and near secondary γ' precipitates for the SC50 sample.

SC200	Primary γ’		Secondary γ’1		Secondary γ’2	
	Atomic %	Error %	Atomic %	Error %	Atomic %	Error %
Ni	61.06	1.08	59.39	2.46	58.90	2.14
Co	8.08	0.60	6.28	0.65	6.63	0.59
Ti	11.33	0.34	8.20	0.75	7.61	0.63
Cr	2.44	0.08	3.07	0.45	2.54	0.36
Al	9.8	0.66	11.34	0.90	11.70	0.80
Nb	3.54	0.41	2.82	0.43	3.17	0.40
Mo	2.74	0.36	5.19	0.59	3.80	0.44
C	0.24	0.03	0.26	0.13	2.00	0.32
W	0.44	0.14	3.33	0.47	2.49	0.35
B	0.24	0.11	0.13	0.09	1.17	0.24

Table 5: The primary and secondary γ’ compositions for the SC200 sample.

SC200	γ near primary γ'		γ far from primary γ'		γ near secondary γ'	
	Atomic %	Error %	Atomic %	Error %	Atomic %	Error %
Ni	42.52	1.45	43.13	1.50	45.69	1.51
Co	15.27	0.78	15.32	0.80	15.51	0.78
Ti	1.91	0.26	2.31	0.29	1.48	0.23
Cr	22.72	0.98	21.14	0.97	22.81	0.98
Al	3.93	0.38	4.58	0.42	3.77	0.37
Nb	2.09	0.27	2.27	0.29	2.02	0.27
Mo	5.11	0.43	6.23	0.49	4.67	0.41
C	1.98	0.27	1.43	0.23	1.23	0.21
W	3.03	0.33	2.38	0.30	1.96	0.26
B	1.43	0.22	1.21	0.21	0.86	0.17

Table 6: The γ compositions near and far from primary γ', and near secondary γ' precipitates for the SC200 sample.

Figure Captions

Fig. 1 (a) and (b) Energy-filtered TEM (EFTEM) images constructed using the Cr M-edge in the EELS spectrum from the solutionized and slow cooled (SC0) sample. The primary and secondary γ' precipitates, which are Cr depleted, exhibit the darker grey contrast in these images.

Fig. 2 (Color online) (a) A 40 nm x 40 nm x 250 nm 3DAP reconstruction of the Al ions (in red) and Cr ions (in blue) from the SC0 sample. The Al-rich region correspond to the primary γ' precipitate and the Cr-rich region correspond to the γ matrix. (b) The same reconstruction showing a cylinder of 5nm diameter, along which a composition profile has been obtained. (c) The corresponding composition profile for Cr, Co, Al, Ti, and Mo ions.

Fig. 3 (Color online) A 50 nm x 50 nm x 40 nm 3DAP reconstruction from the same SC0 sample as in Fig. 2, showing Al ions (in red) and a Cr isoconcentration surface (also referred to in short as isosurface) for Cr = 14at% (in blue). This reconstruction contains a portion of primary γ' precipitate and a number of secondary γ' precipitates.

Fig. 4 (a) and (b) Energy-filtered TEM (EFTEM) images constructed using the Cr M-edge in the EELS spectrum from the solutionized, slow cooled and aged for 50 hrs at 760°C (SC50) sample. The primary and secondary γ' precipitates, which are Cr depleted, exhibit the darker grey contrast in these images.

Fig. 5 (Color online) (a) A 30 nm x 30 nm x 200 nm 3DAP reconstruction from the SC50 sample showing Al ions (in red) and a Cr isoconcentration surface (also referred to in short as isosurface) for Cr = 14at% (in blue). The reconstruction contains a section of a large primary γ' precipitate as well as some sections of smaller secondary γ' precipitates. On it is superimposed a cylinder of 5nm diameter, along which a composition profile has been obtained. (b) The corresponding composition profile for Cr, Co, Al, Ti, and Mo ions.

Fig. 6 (Color online) A 30 nm x 30 nm x 120 nm 3DAP reconstruction from the SC50 sample showing Al ions (in red) and a Cr isoconcentration surface (also referred to in short as isosurface) for Cr = 14at% (in blue). This reconstruction contains substantial portions of secondary γ' precipitates.

Fig. 7 (a) and (b) Energy-filtered TEM (EFTEM) images constructed using the Cr M-edge in the EELS spectrum from the solutionized, slow cooled and aged for 200 hrs at 760°C (SC200) sample. The primary and secondary γ' precipitates, which are Cr depleted, exhibit the darker grey contrast in these images.

Fig. 8 (Color online) (a) (a) A 30 nm x 30 nm x 140 nm 3DAP reconstruction from the SC200 sample showing Al ions (in red) and a Cr isoconcentration surface (also referred to in short as isosurface) for Cr = 14at% (in blue). The reconstruction contains a section of a large primary γ' precipitate as well as some smaller secondary γ' precipitates. On it is superimposed a cylinder of 5nm diameter, along which a composition profile has been obtained. (b) The corresponding composition profile for Cr, Co, Al, Ti, and Mo ions.

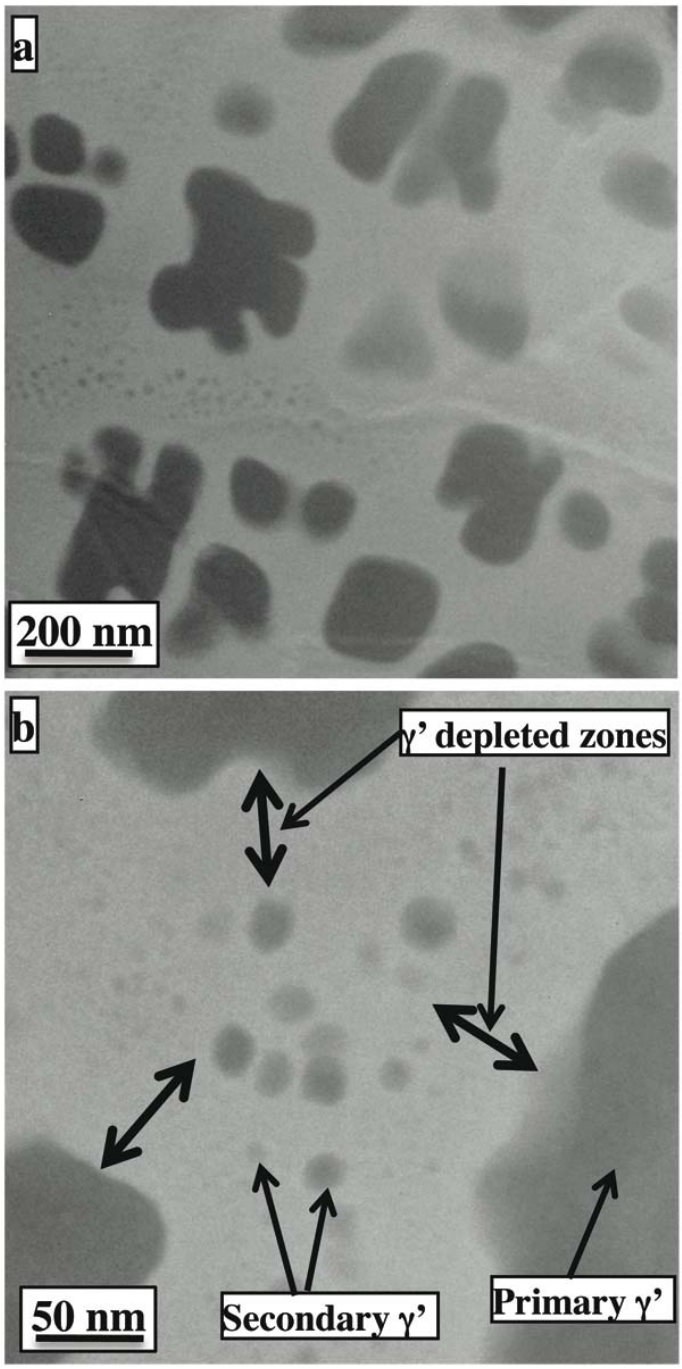

Fig. 1.

a

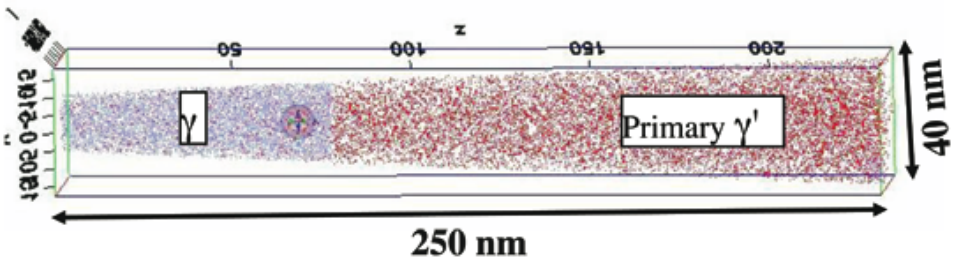
γ
Primary γ'
40 nm
250 nm

b

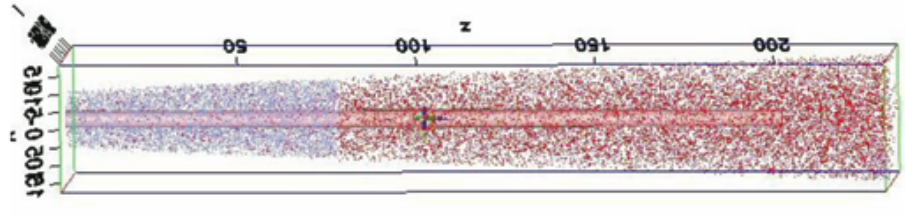

c

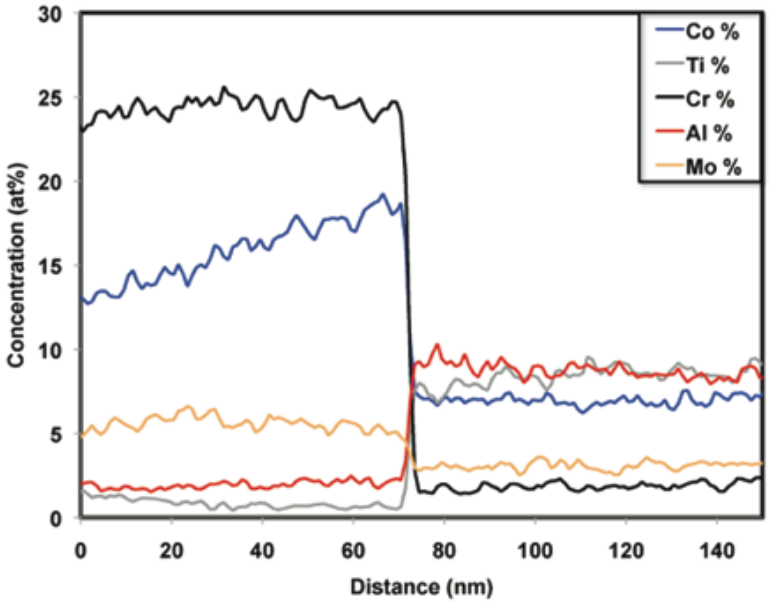
Co %
Ti %
Cr %
Al %
Mo %
Concentration (at%)
Distance (nm)
0
5
10
15
20
25
30
0
20
40
60
80
100
120
140

Fig. 2.

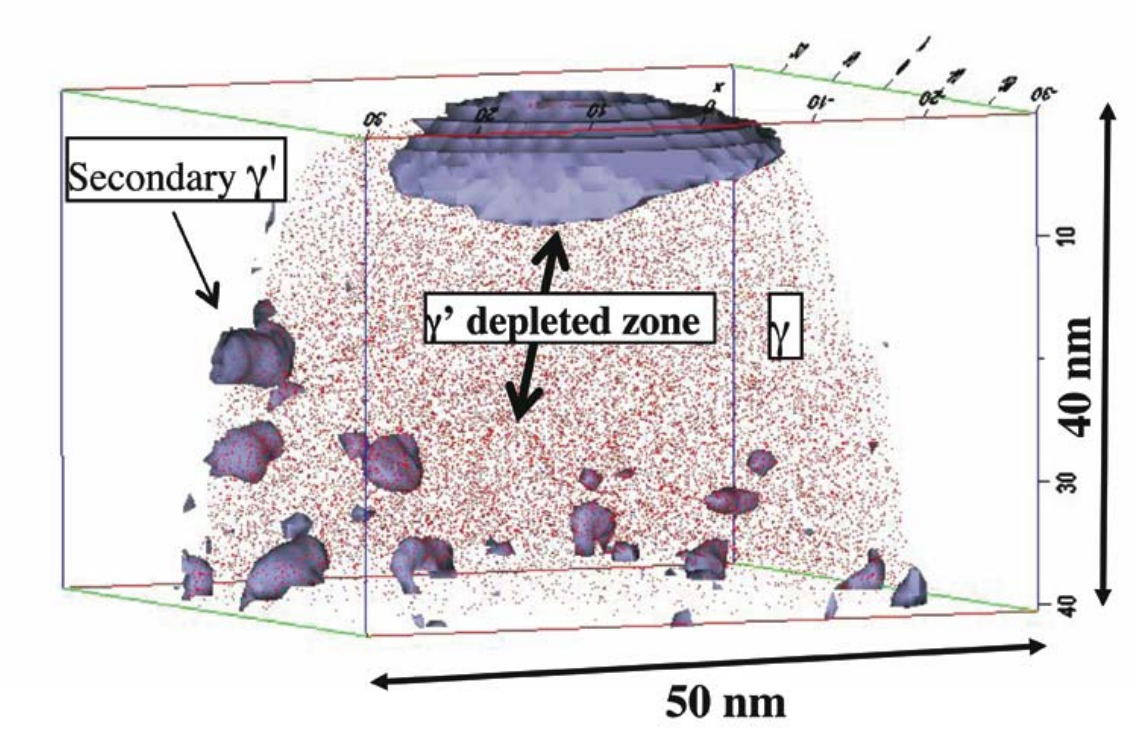

Fig. 3.

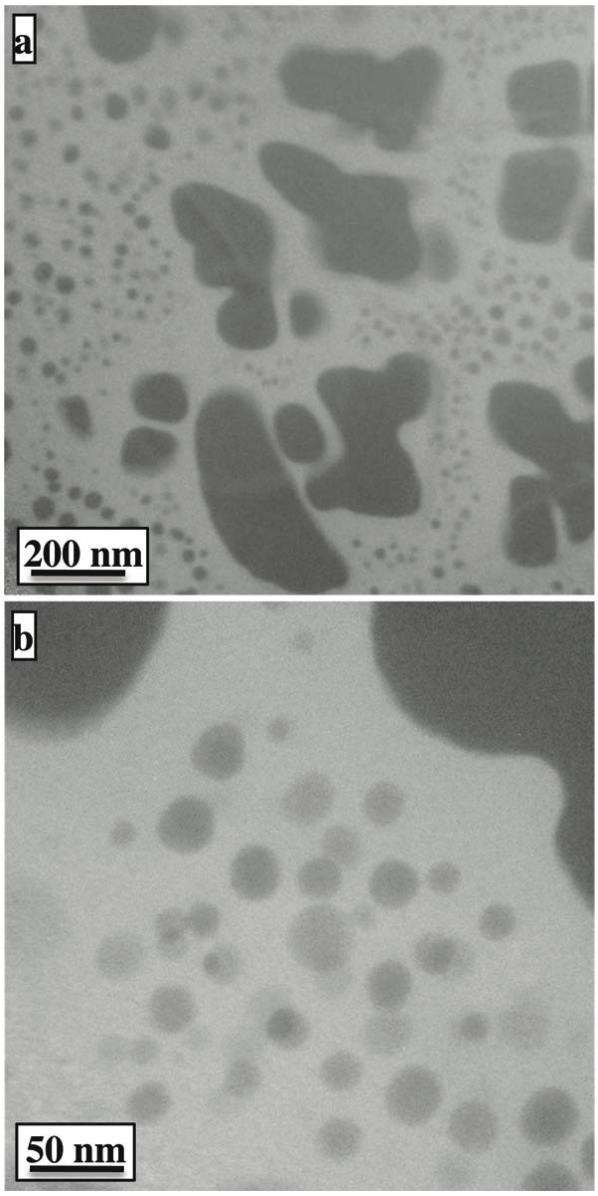

Fig. 4.

a

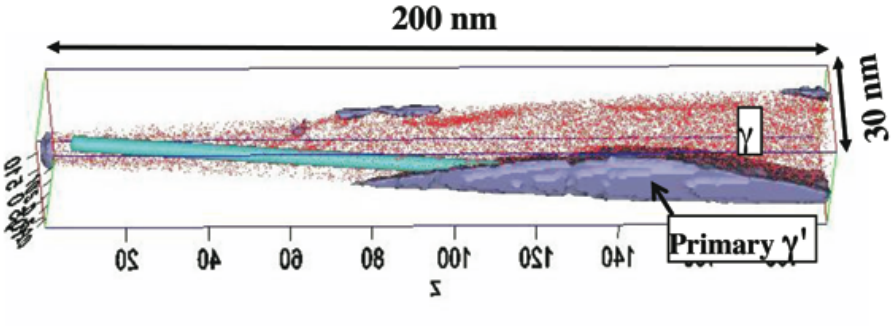
200 nm
30 nm
γ
Primary γ'

b

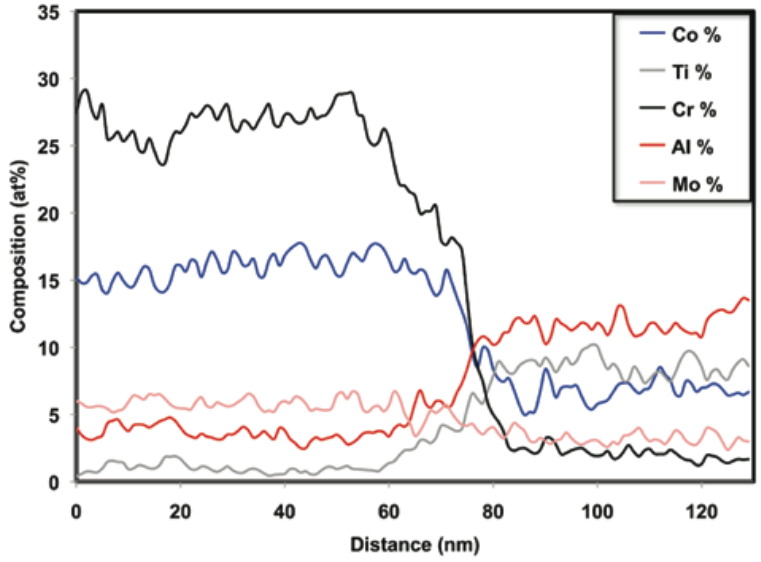
Co %
Ti %
Cr %
Al %
Mo %
Composition (at%)
Distance (nm)
0
5
10
15
20
25
30
35
0
20
40
60
80
100
120

Fig. 5.

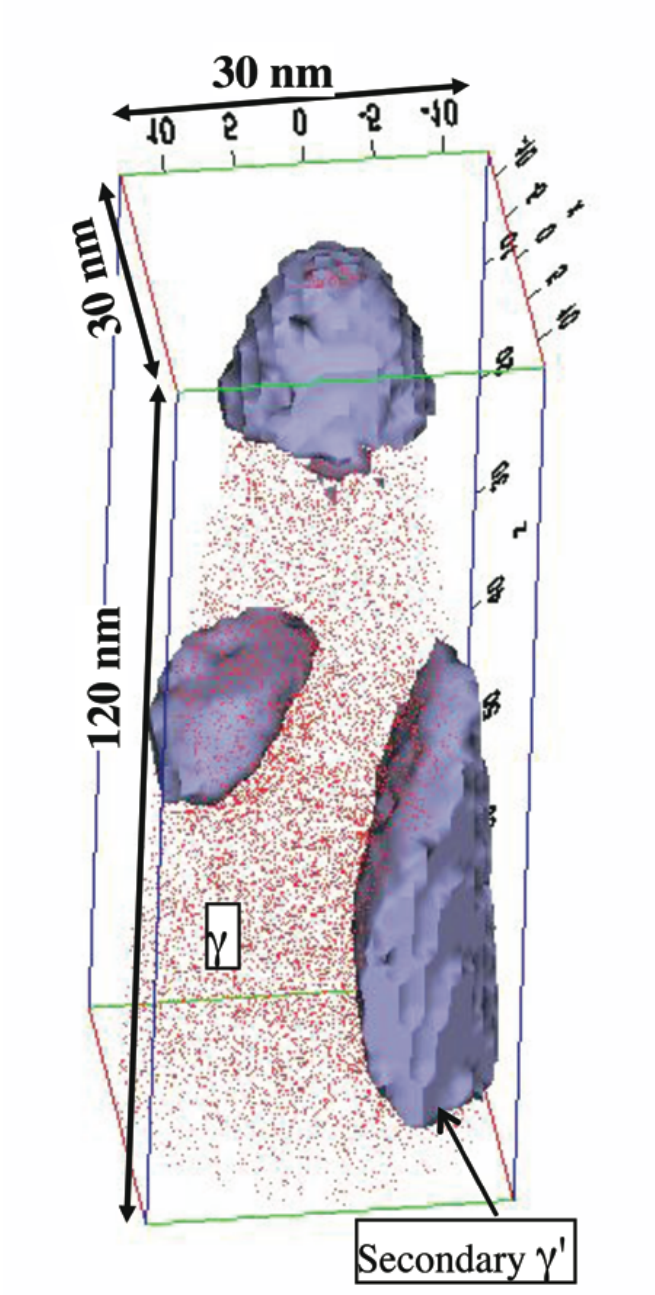

Fig. 6.

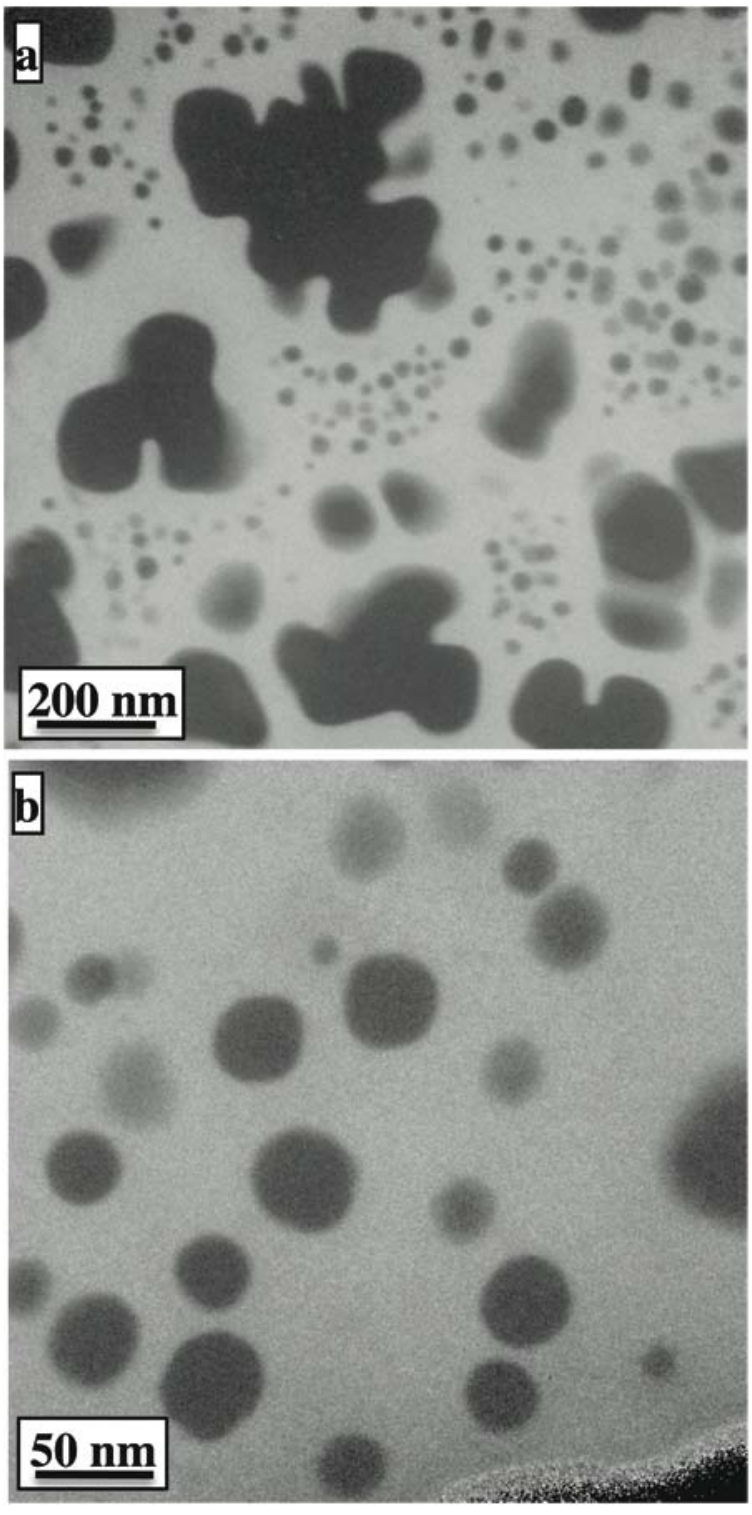

Fig. 7.

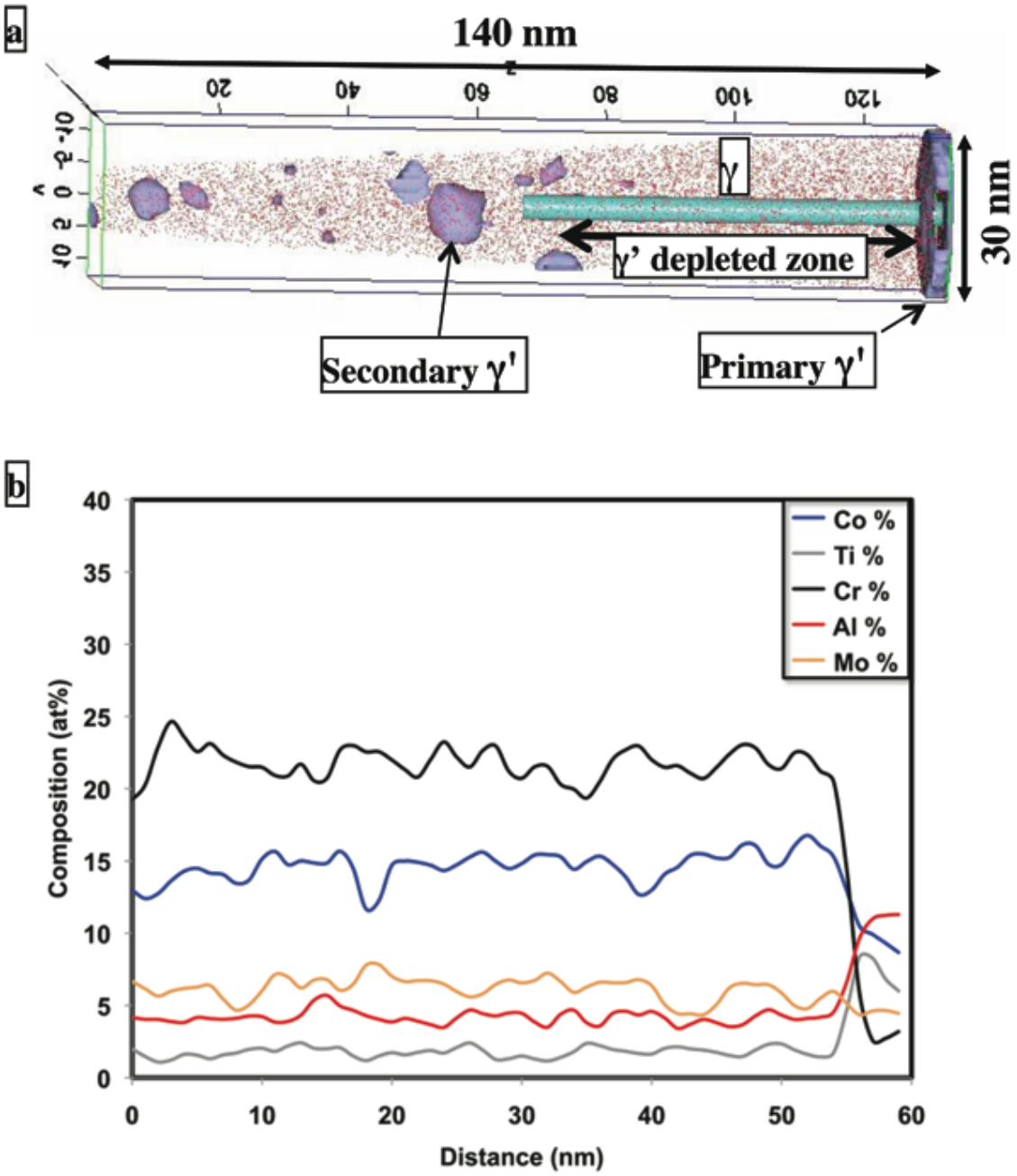
a
140 nm
30 nm
γ
γ' depleted zone
Secondary γ'
Primary γ'
b
Co %
Ti %
Cr %
Al %
Mo %
Composition (at%)
Distance (nm)

Fig. 8.